ELSEVIER

Journal of Power Sources 79 (1999) 262–270

JOURNAL OF POWER SOURCES

The effect of active material loading on the performance of a cylindrical alkaline cell

J.J. Kriegsmann, H.Y. Cheh *

Department of Chemical Engineering and Applied Chemistry, 812 S.W. Mudd, Mail Code 4721, Columbia University, 500 West 120th St., New York, NY 10027, USA

Received 1 February 1999; accepted 7 February 1999

Abstract

The effects of varying the active material loading on the discharge performance of an AA-size Zn/MnO_2 alkaline cell are studied. The active material loading is characterized by two parameters that reflect the weight fraction of solid material removed from the anode and cathode, respectively, in relation to a chosen base case configuration. The anode and cathode loadings are allowed to vary independently of each other. A variety of different capacity ratios are used. Results indicate that the best design is achieved by a specified reduction in the cathode loading, with a balanced amount of the cathode and anode active materials.

Keywords: Alkaline batteries; Active material loading; Porosity; Discharge time

1. Introduction

In a previous study [1], the effect of cathode porosity on the discharge performance of a cylindrical AA-size alkaline cell was examined. Podlaha and Cheh's [2,3] mathematical model of the Zn/MnO_2 system was used to estimate the discharge time by increasing the initial cathode porosity for a given galvanostatic discharge rate and cutoff voltage. Additional cathode void volume was obtained using two methods. The first involved the removal of cathode graphite filler. This was combined with the second technique that changed the internal radii of the cell, so that the cathode thickness was increased while the anode thickness was decreased, thus increasing further the initial cathode porosity. The external geometry of the cell and the active material loading were not altered. The simulations showed that graphite removal significantly increased the discharge time, but the alteration of the internal radii had a much smaller, although still beneficial, effect on performance.

These results indicate that the cathode region and the initial cathode porosity, in particular, are extremely important in determining the cell behavior. It appears as though any additional cathode void volume, which is derived without drastically altering the cell configuration, will enhance the discharge time to some degree. Another procedure that can increase the initial cathode porosity is a reduction of the active material loading. For high-rate discharges the active material utilization is quite low. This leads to the possibility that the active material loading can be reduced without harming the cell life, while simultaneously yielding additional cathode void volume.

There are many investigations where material loading is varied [4–11]. Hwang et al. [4] constructed actual AA-size alkaline cells with different capacity ratios and monitored the discharge behavior under a variety of conditions. Fuller et al. [5], Doyle et al. [6], and Paxton and Newman [7] all varied the material loading when using Ragone plots to determine best designs for the dual lithium ion insertion cell and the nickel/metal hydride cell. In work related to lithium battery systems, Tiedemann and Newman [8], and Newman [9] altered the capacity loading in their analytical models of a porous electrode. Finally, Mao and White [10] and Mao et al. [11] changed the active material level in their models of the Zn/Air and $NiOOH/H_2$ cells, respectively. With the exception of the experimental study [4], all of the analyses [5–11] focused on three main quantities when considering active material loading: electrode capacity, electrode porosity, and electrode thickness.

* Corresponding author. Tel.: +1-212-854-4453; Fax: +1-212-854-3054; E-mail: hyc1@columbia.edu

0378-7753/99/$ - see front matter
PII: S0378-7753(99)00184-6

The goal of this work is to maximize the simulated discharge time for an AA-size Zn/MnO_2 alkaline cell through variations in the active material loading, using an industrially relevant discharge scheme. A methodology is presented for reducing the amount of active material with respect to a selected base case design. Upon determination of the active material amounts yielding the longest discharge time, this system is compared to other AA-size Zn/MnO_2 designs.

2. Active material terms in the theoretical model

Fig. 1 shows a schematic of a cylindrical Zn/MnO_2 alkaline cell, which reflects the one-dimensional, radial geometry. The respective current collector locations for the anode and cathode are given by r_{ac} and r_c. The electrode/separator internal boundary locations are given by r_a and r_s, for the anode and cathode regions, respectively. The cell height is L. The electrodes and the inert separator are porous. The concentrated ternary electrolyte is composed of the two aqueous salts, KOH and potassium zincate, $K_2Zn(OH)_4$. Prior to discharging, the anode solid material contains porous zinc with mercury as an additive, and the cathode solid material is electrolytic manganese dioxide (EMD) with a graphite filler.

In the cathode, EMD is reduced to form manganese oxyhydroxide

$$MnO_2 + H_2O + e^- \rightarrow MnOOH + OH^- \quad (1)$$

In the anode, zinc is oxidized to form zincate ion

$$Zn + 4OH^- \rightarrow Zn(OH)_4^{2-} + 2e^- \quad (2)$$

The zincate ion then precipitates by a homogeneous chemical reaction to form solid zinc oxide

$$Zn(OH)_4^{2-} \rightarrow ZnO + H_2O + 2OH^- \quad (3)$$

Throughout a discharge, the largest amount of precipitation occurs near the anode/separator interface [2].

When active material amounts are changed in an electrode, the porosity of the electrode may also change. However, terms explicitly relating the active material amount and the porosity of an electrode do not appear in the model, for either the anode or cathode. The model equations involving electrode porosity have been discussed in an earlier work [1]. It was argued that increasing the initial cathode porosity would increase the effective electrolyte conductivity and the effective salt diffusivities in the cathode, resulting in a lower polarization loss in the cathode for a particular cell current value.

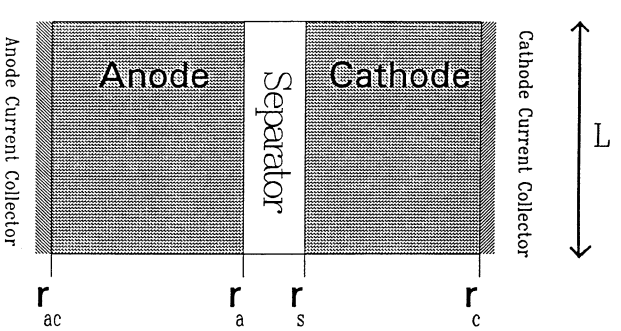

Fig. 1. Schematic for a cylindrical Zn/MnO_2 alkaline cell.

The model assumes that the cell capacity is limited by the cathode reaction. In the anode, the zinc active material mass is not needed in the formulation. A calculation to ensure that the cell capacity is the lower value of the cathode capacity is not present. Thus, there is the possibility of the anode having a lower capacity than the cathode, but the cathode capacity is still chosen as the theoretical cell capacity. This inconsistency will be remedied in a later section.

Cell capacity appears in the depth of discharge calculation. For a galvanostatic discharge, the depth of discharge, f, is given by

$$f = \frac{It}{Q} + f^0 \quad (4)$$

where I is the cell current, t is the time that discharging has taken place, Q is the cell capacity as determined from the cathode, and f^0 is a numerical factor to give an open circuit potential of 1.6 V at the beginning of discharge [12]. The cell capacity is calculated from

$$Q = w_{act,c}\overline{Q}_c \quad (5)$$

where $\overline{Q}_c$ is the specific capacity of EMD assuming a one-electron discharge, and $w_{act,c}$ is the loading level of EMD in the cathode. Faraday's law is used to calculate $\overline{Q}_c$. The above expression for Q assumes a cathodically limited system.

The depth of discharge is an essential quantity in the model. The reason is the dependence of the cell voltage on f. Cell voltage as a function of time is given by

$$E = E_0 + \frac{2RT}{F}\ln\left(\frac{1-f}{f}\right) + \eta(r_a^+) - (\eta(r_a) + \eta(r_{ac})) \quad (6)$$

where E_0 is taken as 1.34 V at the reference state of $f = 0.5$ [2], T is the cell temperature, and the η values refer to the local overpotential evaluated at three different locations in the cell. The first two terms on the right hand side represent the Tye equation for the open circuit potential [13]. Cell voltage will decrease as f rises in value throughout a discharge. The combination of overpotential values also reflect time-dependent voltage losses.

The final appearance of active material terms is with the cathode specific interfacial area, a_c [14]. It is directly proportional to $w_{act,c}$. The cathode specific interfacial area is an influential term in the modified Butler–Volmer electrochemical reaction rate expression for the cathode [2], which governs the transfer current profiles. A large a_c

value lowers the local overpotential throughout the cathode and benefits the cell performance.

3. Optimization strategy

The objective is to find the active material loading in both electrodes that gives the best discharge performance according to Podlaha and Cheh's model for an AA-size Zn/MnO_2 alkaline cell. The selected base case cell configuration and design parameters are identical to those used in Refs. [1] and [2]. The most important system quantities for this work are shown in Table 1. In order to make the results directly comparable with similar studies for this system, a continuous constant current discharge rate of 1.0 A with a 0.8 V cutoff voltage is chosen as the mode of operation, which is also a test condition used in industrial practice [16]. The external cell geometry and the electrode thicknesses are not changed.

In order to increase the initial cathode porosity, a reduction of active material loading is necessary. Relations between active material loading and electrode porosity are not present in the model and must be added. For the greatest generality, the anode and cathode materials should be removable and independently variable of each other. This allows for many different configurations with varying capacity ratios. However, the model must be updated to include the possibility of an anodically limited system, which will alter Eq. (5). Compared to the experimental study [4], simulations can screen a wide variety of designs in a more cost-effective manner.

Active material loading is described by two parameters reflecting the weight fraction of total solid material removed from the anode and cathode. This requires focusing on four quantities in Table 1: $w^0_{act,a}$, the base case zinc amount in the anode, w^0_{Hg}, the base case mercury amount in the anode, $w^0_{act,c}$, the base case EMD amount in the cathode, and w^0_G, the base case graphite amount in the cathode. The new solid material weights are expressed by the two material loading parameters and the base case solid material quantities. The determination of all other relevant input parameters for the model, including electrode capacities and volume fractions, proceed from this step. The best discharge performance is characterized by the longest discharge time for the chosen discharge rate and cutoff voltage.

Table 1
System quantities in the material loading simulations

V_a	2.34 cm^3
V_{sep}	0.23 cm^3 [1]
V_{cath}	3.07 cm^3
Initial KOH concentration	0.007 mol/cm^3 [2]
Initial $K_2Zn(OH)_4$ concentration	5.3×10^{-4} mol/cm^3 [2]
$w^0_{act,a}$	3.71 g [2]
w^0_{Hg}	0.286 g
$w^0_{act,c}$	8.39 g [2]
w^0_G	0.932 g
ρ_{Zn}	6.316 g/cm^3
ρ_{Hg}	13.546 g/cm^3 [15]
ρ_{EMD}	4.370 g/cm^3
ρ_G	2.26 g/cm^3 [15]
ρ_e	1.365 g/cm^3
ϵ^0_s	0.80 [2]
$\overline{Q}_a$	0.820 A h/g Zn
$\overline{Q}_c$	0.308 A h/g MnO_2

4. Active material loading algorithm

The equations needed to determine the input values of $w_{act,a}$, the zinc amount in the anode, w_{Hg}, the mercury amount in the anode, $w_{act,c}$, the EMD amount in the cathode, and w_G, the graphite amount in the cathode, for selected values of the material loading parameters are now presented. Let χ denote the weight fraction of solid material in an electrode that is reduced from the cell loading with respect to the base case design. Thus, χ_a and χ_c refer to reductions in the solid material loading for the anode and cathode, respectively. The parameter χ expresses changes in the cell construction prior to any type of operation or discharging.

The anode solid component weights are calculated from

$$w_{act,a} = (1-\chi_a)\, w^0_{act,a} \tag{7}$$

and

$$w_{Hg} = (1-\chi_a)\, w^0_{Hg} \tag{8}$$

where w^0_{Hg} is determined from base case numbers. Similarly, the cathode solid component weights are computed by

$$w_{act,c} = (1-\chi_c)\, w^0_{act,c} \tag{9}$$

and

$$w_G = (1-\chi_c)\, w^0_G \tag{10}$$

where w^0_G is calculated from base case numbers assuming that the graphite content is 10 wt.% of the total solid material in the cathode [1,17]. From these equations it is clear that when χ_a and χ_c are zero, the base case weights are obtained.

The initial values of the volume fractions in each electrode are now determined. The initial zinc volume fraction in the anode, ϵ^0_{Zn} is given by

$$\epsilon^0_{Zn} = \frac{w_{act,a}}{\rho_{Zn} V_a} = \frac{(1-\chi_a)\, w^0_{act,a}}{\rho_{Zn} V_a} \tag{11}$$

where V_a is the anode volume and ρ_{Zn} is the zinc density, which is chosen to make the base case zinc weight and volume consistent. The initial mercury volume fraction, ϵ^0_{Hg}, is found from

$$\epsilon^0_{Hg} = \frac{w_{Hg}}{\rho_{Hg} V_a} = \frac{(1-\chi_a)\, w^0_{Hg}}{\rho_{Hg} V_a} \tag{12}$$

where ρ_{Hg} is the mercury density. The initial anode porosity, ϵ_a^0, is now calculable, using

$$\epsilon_a^0 = 1 - \epsilon_{Zn}^0 - \epsilon_{Hg}^0 \quad (13)$$

where the initial zinc oxide volume fraction is zero.

The initial EMD volume fraction, ϵ_{EMD}^0, is obtained by

$$\epsilon_{EMD}^0 = \frac{w_{act,c}}{\rho_{EMD} V_{cath}} = \frac{(1-\chi_c) w_{act,c}^0}{\rho_{EMD} V_{cath}} \quad (14)$$

where V_{cath} is the cathode volume and ρ_{EMD} is the EMD density, which is calculated by matching the base case EMD weight and volume under the assumption of 10 wt.% graphite in the cathode material. The initial graphite volume fraction, ϵ_G^0, is found from

$$\epsilon_G^0 = \frac{w_G}{\rho_G V_{cath}} = \frac{(1-\chi_c) w_G^0}{\rho_G V_{cath}} \quad (15)$$

where ρ_G is the graphite density. The initial cathode porosity, ϵ_c^0, is then derived from

$$\epsilon_c^0 = 1 - \epsilon_{EMD}^0 - \epsilon_G^0 \quad (16)$$

where initially there is no manganese oxyhydroxide in the cathode.

The theoretical electrical capacities of each electrode are considered next. The anode theoretical capacity is given by

$$Q_a = w_{act,a} \overline{Q}_a = (1-\chi_a) w_{act,a}^0 \overline{Q}_a \quad (17)$$

where $\overline{Q}_a$ is the specific capacity of zinc, which is also

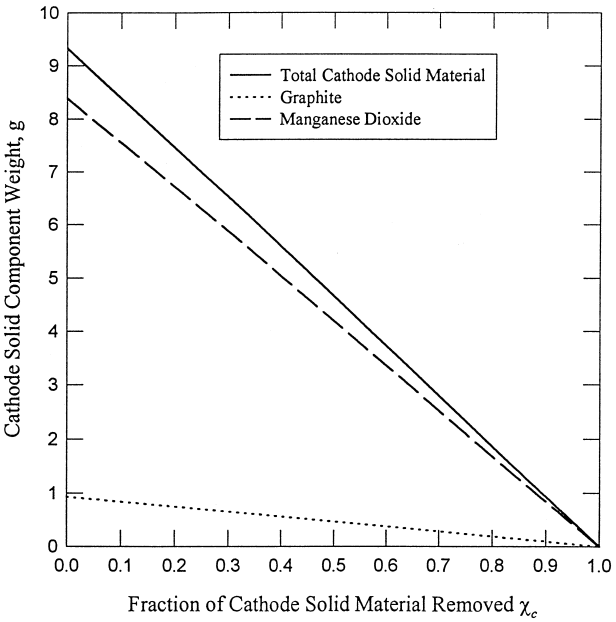

Fig. 3. The dependence of cathode solid component weights on the material loading reduction.

calculated using Faraday's law. The cathode theoretical capacity is computed from

$$Q_c = w_{act,c} \overline{Q}_c = (1-\chi_c) w_{act,c}^0 \overline{Q}_c \quad (18)$$

which is similar in form to Eq. (5), although Q is not necessarily equivalent to Q_c. Eq. (5) is revised by taking the minimum value of Q_a and Q_c as the actual theoretical cell capacity. The new form is

$$Q = \min[Q_a, Q_c] \quad (19)$$

This replaces Eq. (5), and Eq. (4) is still valid. Finally, a

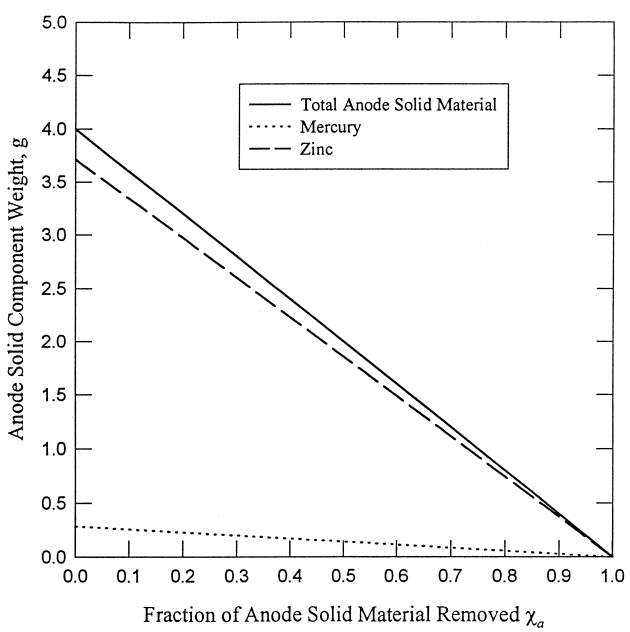

Fig. 2. The dependence of anode solid component weights on the material loading reduction.

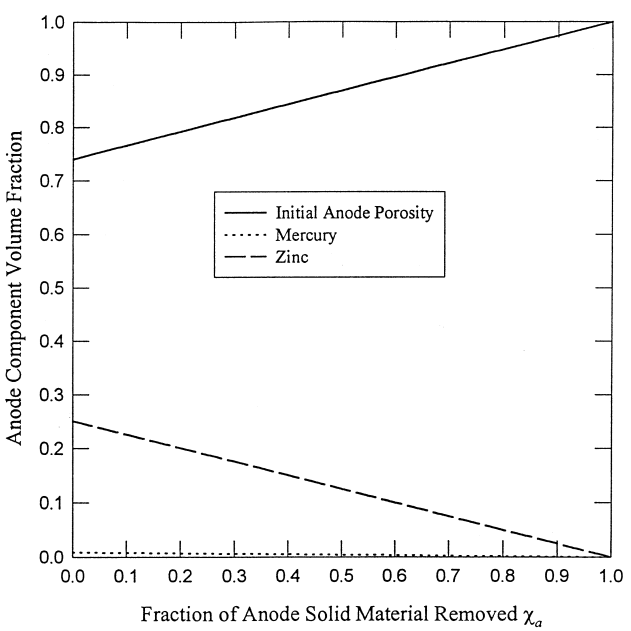

Fig. 4. The dependence of anode component volume fractions on the material loading reduction.

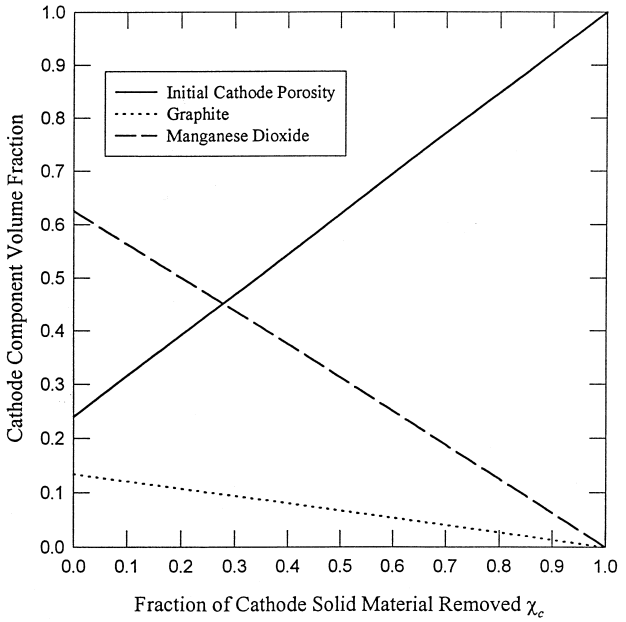

Fig. 5. The dependence of cathode component volume fractions on the material loading reduction.

capacity ratio, Θ, is defined as the cathode to anode ratio of theoretical capacities, or

$$\Theta \equiv \frac{Q_c}{Q_a} = \frac{(1-\chi_c)\, w^0_{act,c} \overline{Q}_c}{(1-\chi_a)\, w^0_{act,a} \overline{Q}_a} \qquad (20)$$

In this sense, a cathodically limited system will have a capacity ratio less than unity, and vice versa.

Figs. 2 and 3 display the electrode component weights in the anode and cathode, respectively, for various reductions in the material loading. The total solid weight in each electrode is included. All component weights approach zero as χ_a and χ_c approach unity. Because of the reaction stoichiometry, the EMD weight is much larger than the zinc weight, and the cathode is considerably more massive than the anode. Figs. 4 and 5 give the corresponding component volume fractions in both electrodes for different loading levels. The base case values are seen when χ_a and χ_c are zero. The electrodes approach porosity values of unity as χ_a and χ_c approach one. Fig. 6 shows the theoretical electrode capacities as a function of material loading reduction. This figure is useful for rapid comparisons of capacity values, including the base case loading.

The algorithm is now included in the numerical solution of the model equations. A pentadiagonal BAND(J) solver [18,19] is used with a modified numerical linearization subroutine [17,20] and the Crank–Nicolson method. The simulations span a range of χ_a and χ_c values under different design schemes.

5. Results

5.1. Material loading reduction in only one electrode

Reduction in the material loading can be investigated one electrode at a time. One of the material loading parameters is set to zero and the other is varied. This reveals which electrode has more of an effect on performance when the loading is reduced. Fig. 7 shows the discharge time to reach the cutoff voltage, t_d, for several cases of solid material removal. It is similar to figures

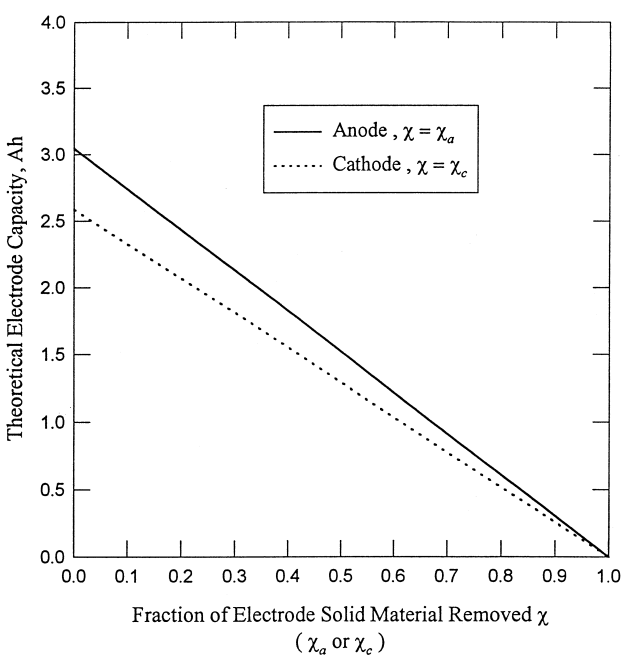

Fig. 6. The dependence of theoretical electrode capacities on the material loading reduction.

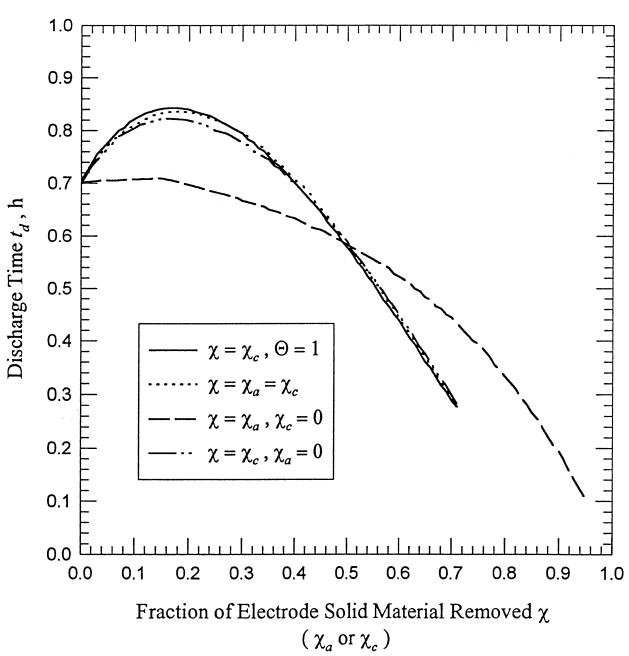

Fig. 7. Discharge time as a function of active material loading for several material reduction schemes.

shown by Evans et al. [21]. For material reduction in a single electrode, the relevant cases are when $\chi = \chi_a$ with $\chi_c = 0$, which signifies anode material reduction, and when $\chi = \chi_c$ with $\chi_a = 0$, which describes cathode material reduction.

A reduction in the cathode loading has a much larger effect on discharge performance than a reduction in the anode loading. The discharge time for the base case with no material removed is 0.700 h. Anode removal reaches a maximum discharge time of 0.709 h when $\chi_a = 0.15$. However, cathode material reduction provides a maximum discharge time of 0.823 h for $\chi_c = 0.16$. This result is in agreement with the results obtained from the cathode porosity study [1]. The initial cathode porosity varies linearly with a reduction in the cathode loading level. Therefore, the optimum χ_c value corresponds to an optimum ϵ_c^0 value, which was the previous finding. The major difference is that the cell capacity is lowered. But the discharge time is indeed raised with respect to the base case. Thus, an appropriate reduction in the loading level is found to benefit the cell performance.

5.2. Equal material loading reduction in each electrode

It is useful to consider the case when the material loading level is reduced equally for each electrode. This keeps the capacity ratio at the base case value, while the cell capacity decreases and the initial electrode porosities increase. The $\chi = \chi_a = \chi_c$ curve in Fig. 7 follows this scenario, and it is represented by $\Theta = 0.850$. This method yields a maximum discharge time of 0.836 h when both parameters are set at 0.18. Anode material removal augments the effect of cathode material reduction and increases the discharge time slightly, relative to cathode material removal alone.

5.3. Material loading reduction with a capacity ratio of unity

A cathodically limited system contains surplus active material in the anode. This is apparent from the base case design and the scheme of equal material loading reduction in each electrode. Reducing this extra amount would not change the cell capacity of a cathode limited design, with a specified χ_c value. However, more initial anode porosity would be obtained and the cell mass will decrease.

To implement this case, Eq. (20) is used with $\Theta = 1$ in order to calculate the χ_a value, for a selected χ_c value, so that the electrode capacities are balanced. The result is

$$\chi_a = 1 - \frac{w^0_{act,c}\overline{Q}_c}{w^0_{act,a}\overline{Q}_a}(1 - \chi_c) \qquad (21)$$

where χ_a is now a function of χ_c. The $\Theta = 1$ curve is shown in Fig. 7. It contains the maximum discharge time compared to the other cases in this figure. At $\chi_c = 0.17$, the maximum discharge time is 0.843 h. This design scheme gives slightly better performance than the case with equal loading level reduction in each electrode.

5.4. Determination of the best design with material loading reduction

A search is performed to find the maximum discharge time, along with the optimum χ_a and χ_c values. The best result is found by setting $\chi_c = 0.17$ and varying χ_a. The maximum discharge time is 0.842 h with $\chi_a = 0.29$. However, this design is almost identical to the best result when $\Theta = 1$, which has a slightly larger discharge time. Both of these cases are shown in Fig. 8, which presents discharge time as a function of electrode material loading reduction. It is concluded that the best design is with $\chi_c = 0.17$ and $\Theta = 1$. Cathode material removal delivers the major performance effect, where anode material removal contributes to a longer discharge time until the cell becomes anodically limited.

5.5. Material loading reduction and the secondary current distribution

In the cathode porosity study, three current distribution parameters [22,23] were analyzed for the cathode region. They included the dimensionless cell current, the dimensionless exchange current density, and the ratio of matrix to electrolyte effective conductivities. These three parameters can also be studied for the case of material loading reduction in each electrode. The parameters in an electrode will all decrease as a result of solid material removal in

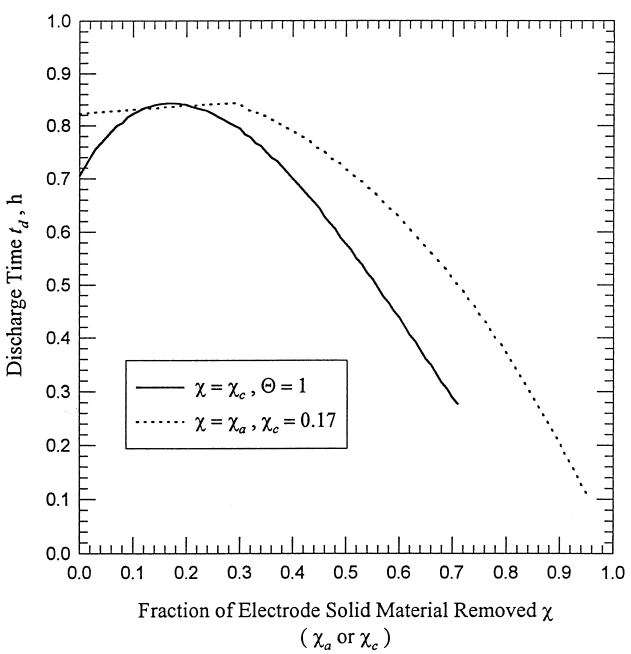

Fig. 8. Determination of the optimum material loading parameters.

that electrode. The transfer current profiles are expected to become more uniform in each electrode as the loading is reduced, and the reactions are shifted away from the electrode/separator interfaces. These calculations are valid only at the beginning of discharge, and the possibility of contact resistance effects is not included.

6. Comparison of cell designs

The best design from the material loading simulations is now compared to the base case and the best configuration from the cathode porosity study. Table 2 lists various quantities for the three systems. The best design from the earlier study has all of the cathode graphite content removed, but the cathode effective matrix conductivity is assumed constant. The depth of discharge value when the cell reaches the cutoff voltage, f_d, is also listed for each case. The active material removal design has a discharge time between the base case and graphite removal designs, representing a 20% increase in cell life with respect to the base case. The graphite removal discharge time gives a 39% improvement in cell life compared to the base case.

The best material loading design achieves the largest utilization of solid reactants, with a final depth of discharge value of about 40%. However, the graphite removal design is very close, with about a 38% depth of discharge. The initial cathode porosity for the material loading design is greater than the graphite removal case, but the material removal scheme has a lower discharge time. It is concluded that the initial cathode porosity is the most important factor that improves the cell performance, as determined in these studies. For fixed electrode thicknesses, the two competing factors relevant to this analysis are the beneficial effect of increasing the initial cathode porosity, as opposed to a lower cell capacity, which results in a higher material utilization in a shorter time [9].

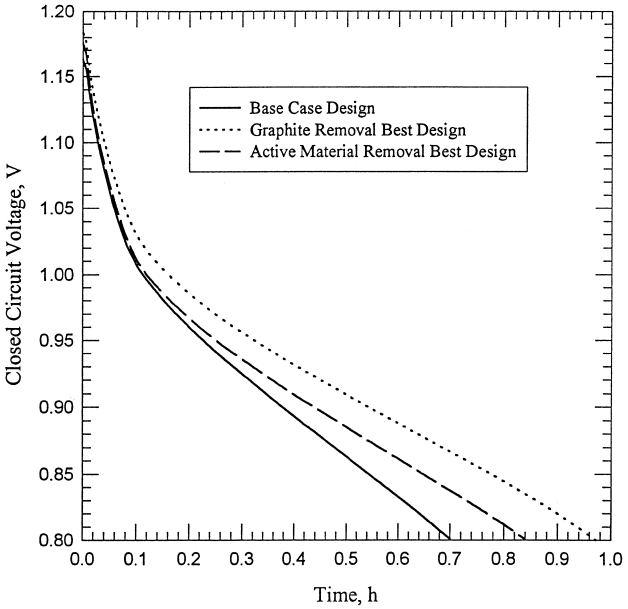

Fig. 9. Cell voltage curves for the three AA-size designs.

Fig. 9 presents cell voltage curves for the three cell designs listed in Table 2. The curves are quite similar until the voltage drops below 1.0 V. The graphite removal design then shows the most favorable operation. The best material reduction design has a performance curve midway between the base case and graphite removal designs.

Finally, these three designs are compared on a broader scale, under a variety of discharge rates, through the construction of Ragone plots. The development given by Doyle et al. [6] is used. Discharges are performed for the three designs by choosing different galvanostatic cell currents with a 0.8-V cutoff voltage. The specific energy and average specific power for each run are computed, and the Ragone plot is made by graphing the specific energy

Table 2
Comparison of design schemes

Quantity	Base case design [1]	Graphite removal best design [1]	Active material removal best design
r_a (cm)	0.43	0.455	0.43
r_s (cm)	0.45	0.474	0.45
χ_a	0	0	0.295
χ_c	0	0	0.170
$w_{act,a}$ (g)	3.71	3.71	2.619
$w_{act,c}$ (g)	8.39	8.39	6.965
w_G (g)	0.932	0	0.774
Q_a (A h)	3.04	3.04	2.147
Q_c (A h)	2.59	2.59	2.147
Θ	0.850	0.850	1.000
ϵ_a^0	0.74	0.765	0.817
ϵ_c^0	0.24	0.320	0.369
M (kg)	0.0236	0.0232	0.0216
t_d (h)	0.700	0.972	0.843
f_d	0.277	0.382	0.399

versus the average specific power. The specific energy, U, is given by

$$U = \frac{1}{M}\int_0^{t_d} EI\,dt \quad (22)$$

where M is the cell mass. The average specific power, P, is then calculated from

$$P = \frac{U}{t_d} \quad (23)$$

The cell mass is computed for each of the three designs by first assuming that the base case design has the default cell mass listed in Ref. [16]. This value is assumed to contain all of the cell components: the electrode solid materials, the separator solid material, the electrolyte, and the rest of the cell—including the current collectors and the cell casing. The extra mass is calculated for the base case and is assumed to be a constant for the other designs, as in Ref. [6]. Any reduction in solid materials is thought to result in additional electrolyte added to the cell, to compensate the increased void volume. The expression is

$$M \times 10^3 = w_{act,a} + w_{Hg} + w_{act,c} + w_G + \rho_e\left[\epsilon_a^0 V_a + \epsilon_s^0 V_{sep} + \epsilon_c^0 V_{cath}\right] + (6.65\,g) \quad (24)$$

where ϵ_s^0 is the initial separator porosity, V_{sep} is the separator volume, and ρ_e is the electrolyte density evaluated with a ternary electrolyte correlation [2], using the initial salt concentrations. Table 1 lists the necessary values. The factor on the left hand side of Eq. (24) is the conversion factor for the correct units, and the numerical constant on the right hand side is the extra mass of the cell components. The cell masses for the three designs are given in Table 2.

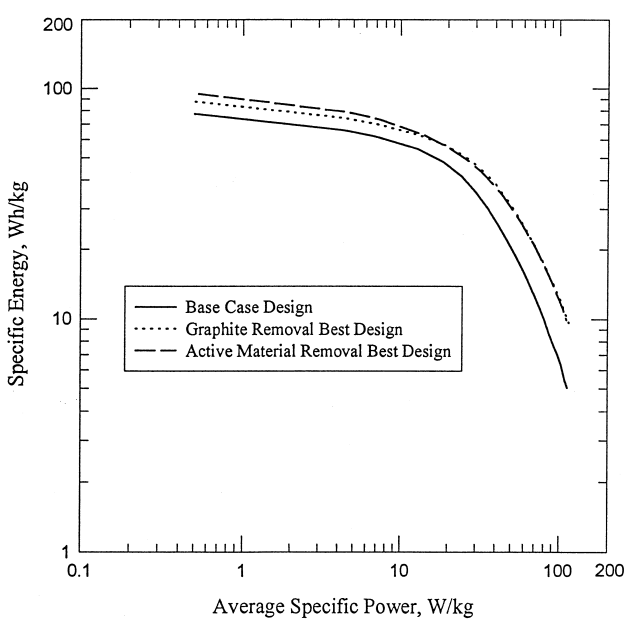

Fig. 10. Ragone plots for the three AA-size designs.

Fig. 10 displays the Ragone plots for the three designs. The curves represent discharge times on the orders of 0.100–100 h. The base case curve lies distinctly below the two other designs, and is thus inferior in terms of the specific energy. For low-rate discharges, the best material removal design has a larger specific energy than the graphite removal design. For high-rate discharges the performance of these two cases is nearly equivalent. The reduced cell mass for the material loading case offsets the lower cell capacity and discharge times in achieving high specific energy values. With each design, the 'knee' region of the Ragone plot [6] lies roughly on the discharge-time line of 1.00 h. The test condition of 1.0 A is in the vicinity of this optimal region for each case. From the Ragone plots, the reduced material loading best design is the superior configuration in this study.

7. Conclusions

When the model is updated to include the dependence of the initial volume fractions and the cell capacity on the solid material amounts, simulations are performed that describe reductions in the active material loading, relative to a base case design. An optimization procedure determines the optimum loading levels of active material in each electrode, so that the discharge time is maximized for a selected galvanostatic discharge rate and cutoff voltage pairing. The best design with active material removal occurs with a specified reduction in the cathode loading such that the cell capacity ratio is unity. This design is compared with the base case design and the best result from the cathode porosity study, which has all graphite filler removed. Although the best active material removal design has a lower discharge time than the best graphite removal design for the test discharge rate, Ragone plots show that the best material removal case is a better system. The best case with active material reduction is more realistic than the graphite removal design, because changes in the cathode effective matrix conductivity were not included in the earlier study.

8. Nomenclature

a_c	specific interfacial area in the cathode (cm^{-1})
E	cell voltage (V)
E_0	open circuit potential after 50% discharge (V)
f	depth of discharge
f_d	depth of discharge at the cell cutoff voltage
F	Faraday's constant (96,487 C/mol)
I	cell current (A)
L	cell height (cm)

M cell mass (kg)
P average specific power (W/kg)
Q theoretical cell capacity (A h)
Q_a anode theoretical capacity (A h)
$\overline{Q}_a$ zinc theoretical capacity (A h/g Zn)
Q_c cathode theoretical capacity (A h)
$\overline{Q}_c$ electrolytic manganese dioxide theoretical capacity (A h/g MnO_2)
r_i current collector location i, or electrode/separator interface location i (cm)
R universal gas constant (8.3143 J/mol K)
t time (h)
t_d discharge time to reach the cutoff voltage (h)
T cell temperature (K)
U specific energy (W h/kg)
V_i volume of component i, or volume of region i (cm^3)
$w_{act,a}$ zinc loading level in the anode (g)
$w_{act,c}$ electrolytic manganese dioxide loading level in the cathode (g)
w_G graphite loading level in the cathode (g)
w_{Hg} mercury loading level in the anode (g)

Greek

ϵ_i porosity of region i, or solid volume fraction of species i
η local overpotential (V)
Θ cathode to anode theoretical capacity ratio
ρ_i density of component i (g/cm^3)
χ weight fraction of electrode total solid material reduced from the cell loading with respect to the base case design
χ_a weight fraction of anode total solid material reduced from the cell loading with respect to the base case design
χ_c weight fraction of cathode total solid material reduced from the cell loading with respect to the base case design

Superscripts

0 with respect to the base case design or initial condition

References

[1] J.J. Kriegsmann, H.Y. Cheh, J. Power Sources 77 (1999) 127.
[2] E.J. Podlaha, H.Y. Cheh, J. Electrochem. Soc. 141 (1994) 15.
[3] E.J. Podlaha, H.Y. Cheh, J. Electrochem. Soc. 141 (1994) 28.
[4] S. Hwang, J. Kim, S.-G. Kim, T. Yeu, Korean J. Chem. Eng. 12 (1995) 146.
[5] T.F. Fuller, M. Doyle, J. Newman, J. Electrochem. Soc. 141 (1994) 1.
[6] M. Doyle, J. Newman, A.S. Gozdz, C.N. Schmutz, J.-M. Tarascon, J. Electrochem. Soc. 143 (1996) 1890.
[7] B. Paxton, J. Newman, J. Electrochem. Soc. 144 (1997) 3818.
[8] W. Tiedemann, J. Newman, J. Electrochem. Soc. 122 (1975) 1482.
[9] J. Newman, J. Electrochem. Soc. 142 (1995) 97.
[10] Z. Mao, R.E. White, J. Electrochem. Soc. 139 (1992) 1105.
[11] Z. Mao, P. De Vidts, R.E. White, J. Newman, J. Electrochem. Soc. 141 (1994) 54.
[12] C.Y. Mak, H.Y. Cheh, G.S. Kelsey, P. Chalilpoyil, J. Electrochem. Soc. 138 (1991) 1607.
[13] W.C. Maskell, J.E.A. Shaw, F.L. Tye, J. Power Sources 8 (1982) 113.
[14] J.-S. Chen, H.Y. Cheh, J. Electrochem. Soc. 140 (1993) 1205.
[15] R.H. Perry, D.W. Green, J.O. Maloney (Eds.), Chemical Engineers' Handbook, 6th edn., Chap. 3, McGraw-Hill, New York, 1984.
[16] Duracell Alkaline–Manganese Dioxide Technical Bulletin, available at http://www.duracell.com/OEM/index.html (select 'Alkaline Manganese Dioxide' link after choosing 'Primary Systems' link).
[17] E.J. Podlaha, PhD thesis, Columbia University, New York, 1992.
[18] J.S. Newman, Electrochemical Systems, 2nd edn., Prentice-Hall, Englewood Cliffs, NJ, 1991, pp. 539–555.
[19] J. Van Zee, G. Kleine, R.E. White, J. Newman, in: R.E. White (Ed.), Electrochemical Cell Design, Plenum, New York, 1984, pp. 377–389.
[20] D.N. Bennion, AIChE Symposium Series 79 (1983) 25.
[21] T.I. Evans, T.V. Nguyen, R.E. White, J. Electrochem. Soc. 136 (1989) 328.
[22] J. Newman, W. Tiedemann, AIChE J. 21 (1975) 25.
[23] M. Doyle, T.F. Fuller, J. Newman, J. Electrochem. Soc. 140 (1993) 1526.